Myosin V Movement: Lessons from Molecular Dynamics Studies of IQ Peptides in the Lever Arm†

Assaf Ganoth, Esther Nachliel, Ran Friedman, and Menachem Gutman*

Laser Laboratory for Fast Reactions in Biology, Department of Biochemistry, George S. Wise Faculty of Life Sciences, Tel Aviv University, Tel Aviv, Israel

Received July 9, 2007; Revised Manuscript Received September 16, 2007

ABSTRACT: Myosin V moves along actin filaments by an arm-over-arm motion, known as the lever mechanism. Each of its arms is composed of six consecutive IQ peptides that bind light chain proteins, such as calmodulin or calmodulin-like proteins. We have employed a multistage approach in order to investigate the mechanochemical structural basis of the movement of myosin V from the budding yeast *Saccharomyces cerevisiae*. For that purpose, we previously carried out molecular dynamics simulations of the Mlc1p−IQ2 and the Mlc1p−IQ4 protein−peptide complexes, and the present study deals with the structures of the IQ peptides when stripped from the Mlc1p protein. We have found that the crystalline structure of the IQ2 peptide retains a stable rodlike configuration in solution, whereas that of the IQ4 peptide grossly deviates from its X-ray conformation exhibiting an intrinsic tendency to curve and bend. The refolding process of the IQ4 peptide is initially driven by electrostatic interactions followed by nonpolar stabilization. Its bending appears to be affected by the ionic strength, when ionic strength higher than ∼300 mM suppresses it from flexing. Considering that a poly-IQ sequence is the lever arm of myosin V, we suggest that the arm may harbor a joint, localized within the IQ4 sequence, enabling the elasticity of the neck of myosin V. Given that a poly-IQ sequence is present at the entire class of myosin V and the possibility that the yeast's myosin V molecule can exist either as a nonprocessive monomer or as a processive dimer depending on conditions (Krementsova, E. B., Hodges, A. R., Lu, H., and Trybus, K. M. (2006) *J. Biol. Chem. 281*, 6079−6086), our observations may account for a general structural feature for the myosins' arm embedded flexibility.

Myosin class V is one of the oldest classes of myosin, being distributed from low eukaryotes, such as yeast, to vertebrate cells. It is the most studied and the best characterized member of the myosin super-family (reviewed in (*1*, *2*)). When bound to actin filaments, myosin V has the ability to convert the energy released by ATP hydrolysis into mechanical work, i.e., movement (*3*). Myosin V is composed of two identical heavy chains that dimerize through a formation of a coiled coil structure to form a homodimer. Each monomer can be divided into an N-terminal head motor domain, an extended neck domain that contains six repeating amino acid sequences called IQ motifs or peptides (designated IQ1−IQ6), and a tail domain containing a coiled coil region attached to a C-terminal globular region. The IQ peptides are ∼25 amino acids segments, centered around the loosely conserved consensus sequence IQxxxR(K)xxxR, and constitute the binding sites for calmodulin (CaM[1]) and CaM-related light chains, such as the Mlc1p protein. Thus, the light chain-binding domain (LCBD) of myosin V is composed of a poly-IQ sequence and six associated light chain-binding proteins (reviewed in (*4*, *5*)).

The current view of how myosin V moves along the actin filament is known as the lever arm mechanism (*6*−*8*). The essence of the proposed mechanism is that nucleotide binding, hydrolysis and product release are all coupled to localized structural transitions within the myosin motor core. These motions are amplified and transmitted to the neck domain, which functions as a lever arm and amplifies them into a large directed translation movement of the entire myosin molecule. Successive alternating cycles of ATP hydrolysis allow the two myosin's motor heads to step along the actin filament toward its barbed end (*9*). Consistent with the lever arm hypothesis is the observation that the myosin's stroke size is proportional to the length of its lever arm (*10*).

The yeast *Saccharomyces cerevisiae* possesses two class V myosins, Myo2p (*11*) and Myo4p (*12*), and both were shown to transport cargo toward the polarized regions of the cell. It is well-established that myosin V from vertebrates is a processive motor (*7*), however the processivity of class V myosins from yeast still remains an unsolved question. Indirect *in vitro* motility assays suggest that it is a nonprocessive motor (*13*), while single molecule *in vivo* microscopy observations indicate that it can exist either as a nonprocessive monomer or as a processive dimer, depending on conditions (*14*).

† This research is supported by the Israel Science Foundation (Grant No. 427/01-1) and the United States−Israel Bi-National Science Foundation (Grant No. 2002129). R.F. acknowledges the Colton Foundation for its support through the Colton Scholarship.

* To whom correspondence should be addressed. E-mail: me@hemi.tau.ac.il. Phone: +972-3-6409875. Fax: +972-3-6409875.

[1] Abbreviations: CaM, calmodulin; LCBD, light chain-binding domain; LJ, Lennard-Jones; MD, molecular dynamics; PDB, Protein Data Bank; PME, particle mesh Ewald; SPC, simple point charge; vdW, van der Waals; VMD, visual molecular dynamics.

10.1021/bi701342y CCC: $37.00
Published on Web 11/20/2007

During recent years, the characteristics of the dynamic motion of myosin over actin filaments have been extensively investigated by various methodologies, such as single molecule fluorescence (*15*−*19*), dark-field (*20*) and electron microscopy (*21*−*24*), mathematical and kinetic modeling (*25*−*29*), and optical trapping (*30*, *31*). These studies suggest a key role to the elasticity of the LCBD during the movement of myosin V. Yet, an atomic resolution description of the neck domain's flexible location has not been exhibited, omitting the structural basis of its flexibility.

Despite the major role of myosins in a wide range of intercellular processes, their structure−function relationship had been previously investigated by rather few molecular dynamics (MD) simulations studies. These simulations were limited to the motor domain in an effort to follow the mechanism of ATP binding and hydrolysis, and were carried out either in the presence of the bound nucleotide (*32*−*39*) or in its absence (*33*, *35*, *38*−*40*). To our knowledge, the neck domain *per se*, being examined in this study, was never subjected to MD simulations.

The whole length of the lever arm is too large for MD simulations due to limitations of computational power. Thus, we focus our simulations on two of its discrete building blocks, the IQ peptides and their counterparts CaM-like proteins. Accordingly, in previous studies (*41*, *42*), we used MD simulations to investigate the dynamics of the Mlc1p−IQ4 and the Mlc1p−IQ2 protein−peptide complexes from the budding yeast *Saccharomyces cerevisiae* myosin class V Myo2p. We have noticed that upon release from its crystal constraints, the Mlc1p−IQ4 complex experienced a major conformational rearrangement during MD simulations. The Mlc1p protein had lost its dumbbell-like extended shape and was transformed into a collapsed form, which tightly engulfed the IQ4 peptide. In parallel, the IQ4 peptide did not keep its rodlike structure and became bent. Yet, the MD-derived structure of the Mlc1p−IQ2 complex was close to its X-ray one, whereas both the Mlc1p protein and the IQ2 peptide retained a stable straight configuration. Comparison of the two Mlc1p−IQ complexes revealed a higher similarity in their simulated configurations than that presented by their crystal structure states. A progression toward a relatively common compact shape of the protein was observed as the configurations of the two protein−peptide complexes evolved along their MD trajectories.

To evaluate whether the tendency of the IQ4 peptide to refold is embedded in the Mlc1p−IQ4 protein−peptide complex or an innate feature of the peptide itself, we carried out long duration (total of 0.47 μs) MD simulations of free IQ2 and IQ4 peptides from the budding yeast *Saccharomyces cerevisiae* myosin class V Myo2p in various conditions. The results demonstrate that the IQ2 peptide keeps an extended elongated conformation in solution, whereas the IQ4 peptide bends. The bending of the IQ4 peptide appears to be controlled by the salt concentration of its buffer solution, when high ionic strengths (∼300 mM and above) preclude it from flexing. The IQ4 peptide refolding process is initially driven by electrostatic interactions followed by nonpolar stabilization. When the IQ4 peptide is elongated by 10 additional amino acids flanking each of its terminals (representing an enlarged fraction of the LCBD), its inherent tendency to curve was observed as well. Finally, by addressing MD-derived stable conformations of two neck Mlc1p−IQ complexes (*41*, *42*), the kinetic energy obtained by ATP hydrolysis from the head domain (*32*), the possibility that the yeast myosin V can exist either as a nonprocessive monomer or as a processive dimer (*14*), and the MD simulations of free IQ2 and IQ4 peptides reported in this study, we present a functional dynamic model of the LCBD of myosin V from the budding yeast *Saccharomyces cerevisiae*. We suggest that the intrinsic plasticity of the IQ4 peptide provides the lever arm with a joint flexible elbow that, despite its tight interaction with the Mlc1p protein, assists to the proper function of myosin V.

MATERIALS AND METHODS

MD Simulations. The IQ2 Peptide. The MD simulations were performed using the GROMACS 3.2.1 package of programs (*43*−*45*), with the GROMOS96 43a1 force field (*46*). The coordinates for the IQ2 peptide were derived from the crystal structure of its complex with the Mlc1p protein (PDB file 1M45), determined by X-ray crystallography at 1.65 Å (*47*), that was downloaded from the Protein Data Bank (*48*). The protein−peptide complex was embedded in a box containing the SPC water molecules (*49*), that extended to at least 12 Å between the peptide's structure and the edge of the box. Assuming normal charge states of ionizable groups corresponding to pH 7, the net charge of the IQ2 structure is +2e. Hence, 13 sodium and 15 chloride ions were added to the simulation box at random positions, to neutralize the system at a physiological salt concentration of ∼100 mM. Prior to the dynamics simulation, internal constraints were relaxed by energy minimization. Following the minimization, an MD equilibration run was performed under position restraints for 40 ps. Then, an unrestrained MD run was initiated. The first 100 ps of the run was treated as a further equilibration simulation, and the remainder 100 ns was saved and used for the analysis. During the MD run, the LINCS algorithm (*50*) was used in order to constrain the lengths of all bonds; the waters were restrained using the SETTLE algorithm (*51*). The time step for the simulation was 2 fs. The simulation was run under NPT conditions, using Berendsen's coupling algorithm for keeping the temperature and the pressure constant (*52*) ($P = 1$ bar; $\tau_P =$ 0.5 ps; $\tau_T = 0.1$ ps; $T = 300$ K). Van der Waals (vdW) forces were treated using a cutoff of 12 Å. Long-range electrostatic forces were treated using the PME method (*53*). The coordinates were saved every 1 ps.

The IQ4 Peptide. The coordinates for the IQ4 peptide were derived from the crystal structure of its complex with the Mlc1p protein (PDB file 1M46), determined by X-ray crystallography at 2.1 Å (*47*), that was downloaded from the Protein Data Bank (*48*). The technical details of the simulations were similar to those described for the IQ2 peptide. The MD simulations were performed under various conditions as elaborated in Table 1. The net charge of the IQ4 peptide is +6e, whereas the number of ions that were added at the simulations varied according to the specific conditions of each simulation.

Visual Presentations. All protein figures were created using the VMD computer program (*54*).

Lennard-Jones Interactions. Lennard-Jones (LJ) interactions were computed using a standard GROMACS utility.

Electrostatic Interactions. Short-range electrostatic interactions were computed by using a standard GROMACS utility

Table 1: Summary of the MD Simulations of the IQ4 Peptide

	duration (ns)	concn of salt	no. of added Na^+ ions	no. of added Cl^- ions
IQ4 peptide	100	~100 mM	12	18
IQ4 peptide[a]	30	~100 mM	12	18
extended IQ4 peptide[b]	20	~100 mM	10	17
IQ4 peptide[c]	20	~30 mM	4	10
IQ4 peptide[d]	100	~300 mM	36	42
IQ4 peptide[e]	100	~2.4 M	288	294

[a] High temperature (400 K). [b] An IQ4 peptide containing 10 additional amino acids flanking each of its terminals was built using Swiss PDB Viewer (*78*). These added 20 residues belong to the IQ3 and IQ5 peptides. Thus, the 45 amino acid elongated IQ4 peptide constitutes a portion of the poly-IQ sequence as present at the neck of the myosin. [c] Low salt concentration. [d] High salt concentration. [e] Very high salt concentration (mimicking the salt concentration in which the Mlc1p−IQ4 protein−peptide complex was crystallized (*47*)).

with cutoff of 12 Å. To make sure that the calculations are also valid for longer ranges, they were repeated with cutoffs of 14, 16, 18, and 20 Å. This did not affect the trend of the results.

Free Energy Profile. Given a system in thermodynamic equilibrium, the change in free energy upon transformation from a reference state, (*ref*), of the system to another generic state, (*i*), (e.g., from folded to refolded), at constant temperature and constant pressure, can be evaluated as

$$\Delta G_{\mathrm{ref}\rightarrow i} = -RT \ln \frac{p_i}{p_{ref}} \qquad (1)$$

where R is the ideal gas constant, T is the temperature, and p_i and p_{ref} are the probabilities (obtained by the MD simulation) of finding the system in state (*i*) and state (*ref*), respectively. Any global parameter can be used to evaluate the free energy, such as the radius of gyration, atomic RMSD, or fluctuations along principal components (*55*−*61*). In the present study, we use the free energy surface as a function of the gyration radius of the IQ4 peptide.

RESULTS

Overall Conformational Changes during the Simulations. The simulated structures of the IQ2 peptide, as it varies from its crystal structure with time, are presented in Figure 1 by snapshots taken at 20 ns intervals. At its initial configuration, the IQ2 peptide is an almost linear α-helix. Within the first 20 ns of simulation, both its N- and C-termini loosen, while its mid-section retains a straight conformation. During the rest of the simulation up to 100 ns, the structure of the peptide hardly changes, reflecting its stable MD-derived configuration. However, subtle reversible conformational modifications may occur, as can be seen at the 60 ns snapshot.

In contrast to the rigidity of the IQ2 peptide, snapshots taken from the trajectory of the IQ4 peptide reveal a different scenario (Figure 2A). The initial configuration of the IQ4 peptide, as extracted from the Mlc1p−IQ4 protein−peptide complex X-ray structure, is a linear α-helix. After only 20 ns of simulation, its conformation grossly deviates from its initial one. Its C-section loses the straight conformation, and modulates into turn and bent structures. The conformation of the IQ4 peptide continues to explore the configurational space till reaching a new configuration, represented by the following snapshots. At this newly gained conformation, the IQ4 peptide is refolded in a manner that its N- and C-termini are relatively close to each other, having the shape of two helices separated by a coiled hinge. Since the IQ4 peptide bears eight positive and two negative residues, it seems likely that its refolded conformation is stabilized by internal salt bridges. Hence, we followed the minimal distance between pairs of its positive and negative residues as a function of time, and present these that formed intrapeptide salt bridges (Figure 2B). As shown in Figure 2B, at the beginning of the simulation, residues K11−E25 (black) and R4−E25 (gray) are apart from each other. For both cases, at $t \sim 65$ ns, the distance between the residues sharply drops from >1 Å to a distance in which their atoms almost reached to a contact of their vdW radii ($d = 2.5$ Å). The approach of these residues toward each other is a relatively slow process, ranging tens of nanoseconds, that seems to be stable till the simulation was terminated. Interestingly, the refolding of the peptide involves an increase of the distance between positive residues located on its mid-section (Figure 2C). The K12−K15 (black) and the R14−K18 (gray) distances increase as the simulation proceeds. The distribution of the positively charged residues along the peptide causes an electrostatic repulsion that rejects them from each other, and consequently the peptide refolds and loses its extended helical conformation. The role of the electrostatic potential of the peptide is further evaluated below.

To validate that the structure of the IQ4 peptide at 100 ns reflects a representative stable conformation, we repeated the simulation of the IQ4 peptide at a high temperature (400 K) for 30 ns, and the last snapshot of that simulation is shown in Figure 2A (bottom, right). Inspection of the peptide's structure at the end of the 400 K simulation reveals a high similarity to the structure gained at 300 K, presenting an innate capacity to flex. The refolding mechanism of the peptide, at both temperatures, was similar to that observed by MD simulations of the Mlc1p−IQ4 protein−peptide complex at different temperatures (*41*).

To evaluate the energy changes involved with the structural modulation process undergone by the IQ4 peptide, we calculated its nonpolar, i.e., Lennard-Jones (LJ), and short-range Coulomb electrostatic energies (Figure 3A and 3B, respectively). Both terms decreased, though in different manners, as a function of the simulation time. The stability generated by the nonpolar interactions is ~50 kJ/mol, taking place at a discrete time point, after which its value is practically constant. The short-range Coulombic energy contributes ~200 kJ/mol, but appears to gradually evolve over most of the simulation time. It is of interest to point out that the initial deformation of the peptide's α-helical structure is driven by electrostatic interactions of the charges residues, either among themselves or with the solvent.

The energy of a protein is a function of the topological arrangement of its N atoms and their interactions with the solvent. In exact terms, it is described by a hyper-surface in the $3N$-dimensional configurational space, with a very large number of minima separated by activation barriers and saddle points. Each valley in this hyper-surface pertains to a particular conformation of the protein (*62*, *63*). Due to the high dimensionality of the configurational space of a protein, it is impossible to give a representative picture of its free energy landscape as a function of the entire phase space. To

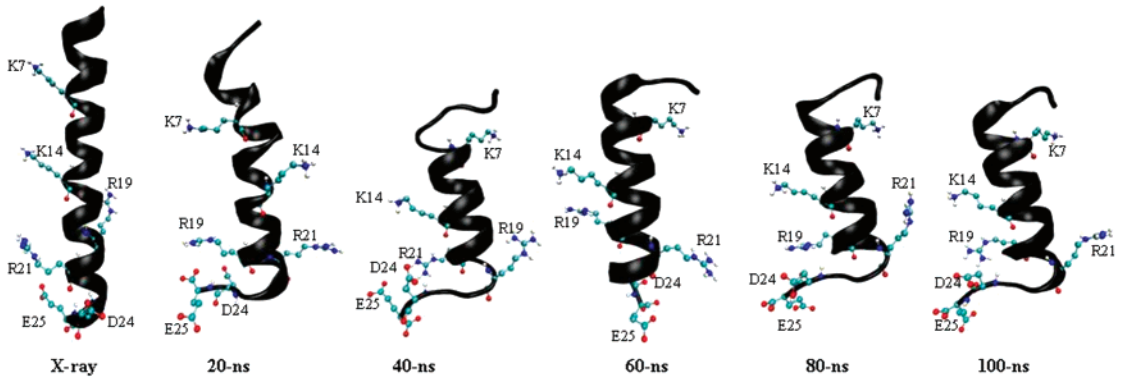

FIGURE 1: The crystal structure of the IQ2 peptide, and snapshots from its simulation, taken at 20-ns intervals. Charged residues (K7, K14, R19, R21, D24 and E25) are shown as indicatives.

overcome this problem, we represent the energy profile in a lower dimensional subspace by using a global parameter (here, the gyration radius), which allows the identification of ensembles of subconformations belonging to a given structural state. Thus, to correlate the stability of the peptide with its conformation, we calculated its free energy profile as a function of the gyration radius (R_g) (Figure 3C). The probability that the peptide may assume a refolded compact configuration is higher than it may hold an extended structure. Since these probabilities are directly linked to the free energy (see Materials and Methods for details), the analysis suggests that the peptide's simulated structure after 100 ns of simulation is energetically more stable than its crystal structure. As seen in Figure 3C, the upper and lower limits of the R_g confine the conformational space, which is found at the range of 7.8 Å $\leq R_g \leq$ 11.7 Å. Within this range, the peptide exhibits three populations, having minima at $R_g \sim$ 11.5 Å, 9.7 Å and 8.1 Å. Among these populations, which are separated by energy barriers, the most stable one persists at $R_g =$ 8.1 Å. Considering the steepness of the curve on both edges of the ordinate, it is unlikely that the peptide will probe structures that are outside the charted range. Evidently, the MD-derived conformation is characterized by an energetic minimum.

We wish to stress out that a two-dimensional representation of a high-dimensional hyper-surface, as the free energy landscape of a peptide, is highly degenerate. This means that what appears in Figure 3C as a well-defined minimum may be a result from a superposition of a series of minima that cannot be resolved. Moreover, due to computational power limitations the conformational sampling is rather limited and, as such, imperfect. Therefore, the numerical values on the ordinate should be taken as indicative, representing qualitative trends rather than actual quantitative ones. Yet, the presentation allows the identification of energy wells that correspond to temporally and structurally distinct subsets of structures visited during the simulation.

Secondary Structure Analysis of the IQ Peptides. The structural transformations of the IQ2 and the IQ4 peptides are shown by their secondary structure analysis, depicted in Figure 4. This analysis enables detection of subtle changes in the secondary structure composition, which are not necessarily observed by discrete snapshots. The secondary structure analysis of the IQ2 peptide (Figure 4A) reveals that its initial α-helical conformation remains stable for more than 20 ns. Then, it transforms into a 5-helix conformation, while keeping its linearity. The 5-helix conformation survives during the rest of the simulation with few events of reappearance of an α-helix (such as the time interval stretch of 32 ns to 36 ns).

The secondary structure analysis of the IQ4 peptide (Figure 4B) exhibits a different pattern. After a short relaxation period, the IQ4 peptide is no longer composed of only α-helical elements. While its first ~15 residues still keep their α-helical configuration, the remaining residues become composed of a mixture of bends and turns. At ~16 ns, a 5-helix appears and gradually controls over the structure until ~38 ns (besides a middle coil/turn section). Apparently, the 5-helix conformation is not stable enough for the given sequence to persist for the entire helix, and is replaced by an α-helical conformation that holds for the N-section. From this time point on, the structure of the peptide exhibits three secondary structure elements, reflecting an energetically stable configuration: an N-section, composed of an α-helix; a C-section, composed of a 5-helix; and a hinge, composed of turn and coil, separating between these N- and C-sections.

It should be noted that the α- to 5-helix transition (full-length and partial for the IQ2 and the IQ4 peptides, respectively), which was detected in both simulations, was observed, as well, in several other MD simulations. For example, 5-helix propagation at the expense of an α-helix was evidenced in simulations of the trans-membrane domain of ErbB-2 (*64*, *65*), the central domain of caldesmon (*66*) and some synthetic peptides (*67*).

The Effect of Salt Concentration on the MD-Derived Structure of the IQ4 Peptide. The MD simulations of the IQ4 peptide, either in a complex with the Mlc1p protein (*41*, *42*) or as a free peptide suggest that its preferential configuration is bent. However, the crystal structure of the Mlc1p−IQ4 complex recorded a straight rodlike conformation for the peptide. This discrepancy may stem from the very high salt concentration used for the crystallization (~2.4 M) (*47*). To account for that, we investigated the effect of salt concentration on the structure of the IQ4 peptide. We performed MD simulations in three different salt concentrations: ~30 mM (low), ~300 mM (high) and ~2.4 M (very high). The durations of the simulations were 20 ns, 100 ns and 100 ns, respectively. The last snapshot, which in all cases represents the dominant structure, is shown in Figure 5.

At the low (Figure 5, left) and the medium (~100 mM, as elaborated in the previous sections) ionic strengths, the IQ4 peptide spontaneously refolded into two distinctive

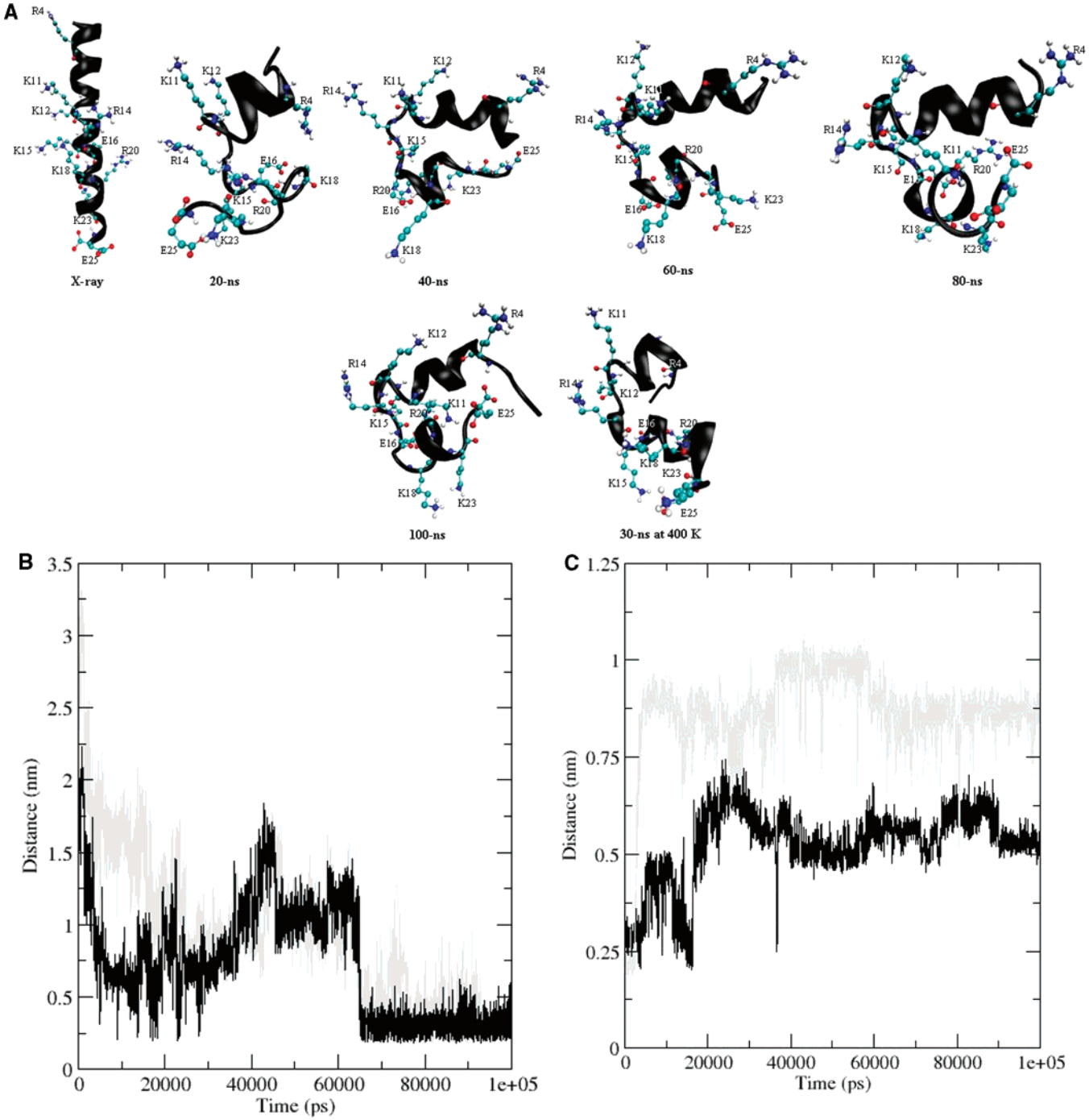

FIGURE 2: (A) The crystal structure of the IQ4 peptide; snapshots from its simulation at 300 K, taken at 20-ns intervals; and the last snapshot form its simulation at 400 K. Charged residues (R4, K11, K12, R14, K15, E16, K18, R20, K23 and E25) are shown as indicatives. (B) Intrapeptide salt bridges as a function of the simulation time. Minimal distance between residues K11 and E25 (black), and between residues R4 and residue E25 (gray). (C) Minimal distance between residues K12 and K15 (black), and between residues R14 and residue K18 (gray) as a function of the simulation time.

sections separated by a hinge. At the very high salt concentration that mimics the crystallization buffer liquor, the peptide did not refold, although its N- and C-termini loosened (Figure 5, right).

Most likely, high salt concentrations prevent the peptide from assuming a conformation that reflects its stable MD-derived structure, keeping it as an elongated nonphysiological helical rod. Given that the peptide hardly bends at the high salt concentrations (as opposed to the bending at ~30 mM and ~100 mM salt concentrations), its refolding pattern is obviously influenced by the concentration of ions in its surrounding. This was confirmed by a residue-level salt bridge analysis, in which we found that intrapeptide salt bridges did not form at salt concentrations of ~ 300 mM and above. At such concentrations, the charged residues of the peptide are adequately solvated by the ions, allowing the peptide helix to be elongated. The effect of the screening electrolyte on the structure of the peptide can be also evaluated by referring to the Debye length of the solution. At ~30 mM and ~100 mM, the electrolyte does not effectively screens charges, and the Debye length is relatively large. Thus, at these concentrations, the positive charges on

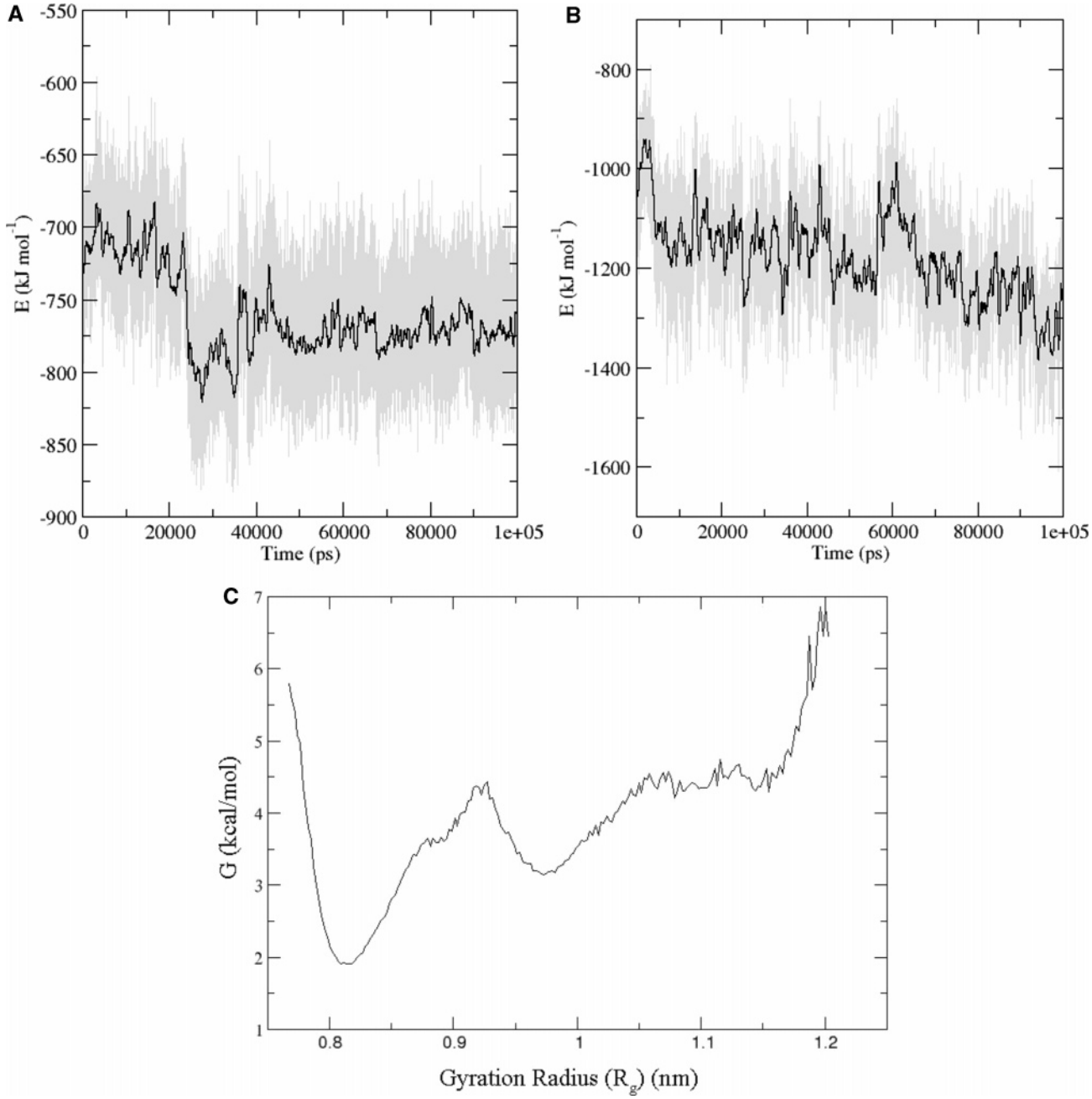

FIGURE 3: (A) The Lennard-Jones component of the potential energy among the residues of the IQ4 peptide (gray), and its averaged values every 250 ps (black). (B) The short-range electrostatic interactions among the residues of the IQ4 peptide (gray), and averaged values every 250 ps (black). (C) Free energy projection over the gyration radius (R_g) of the IQ4 peptide.

the peptide effectively repel each other, and its refolding may take place (see Figure 2C). At 300 mM and above, the screening length is short-ranged, and hence the positively charged residues can tolerate the presence of other similarly charged residues, suppressing the peptide's refolding.

The conformation of the peptide at ~2.4 M resembles the one obtained by the simulation at the high salt concentration (Figure 5, middle) because already at ~300 mM NaCl the screening effect caused by the ions is extensive. According to our observation, the 8-fold increase at the NaCl concentration did not significantly enhance the screening effect, and thus the results of the high and the very high salt concentrations' simulations are similar.

Structure and Dynamics of an Extended IQ4 Peptide. In order to verify that the kink presented by the IQ4 peptide (Figure 2A) is not an artifact caused by its exposed N- and C-termini, we built an extended IQ4 peptide that was then studied by a 20 ns MD simulation. The sequence of this extended peptide consisted of that of the IQ4 peptide, as present at the crystal structure of the Mlc1p−IQ4 complex, supplemented by additional twenty residues; ten of these residues flank its N-terminus and are part of the IQ3 peptide sequence, while the other ten reside after its C-terminus and belong to the IQ5 peptide sequence. Hence, the 45 amino acid long sequence represents a fair section (~30%) of the full-length poly-IQ (IQ1−IQ6) neck of myosin V.

The secondary structure analysis of the extended IQ4 peptide (Figure 6) demonstrates that it experiences a similar refolding pattern as observed for the IQ4 peptide. Its N-section retains a rigid structure; whereas its C-section

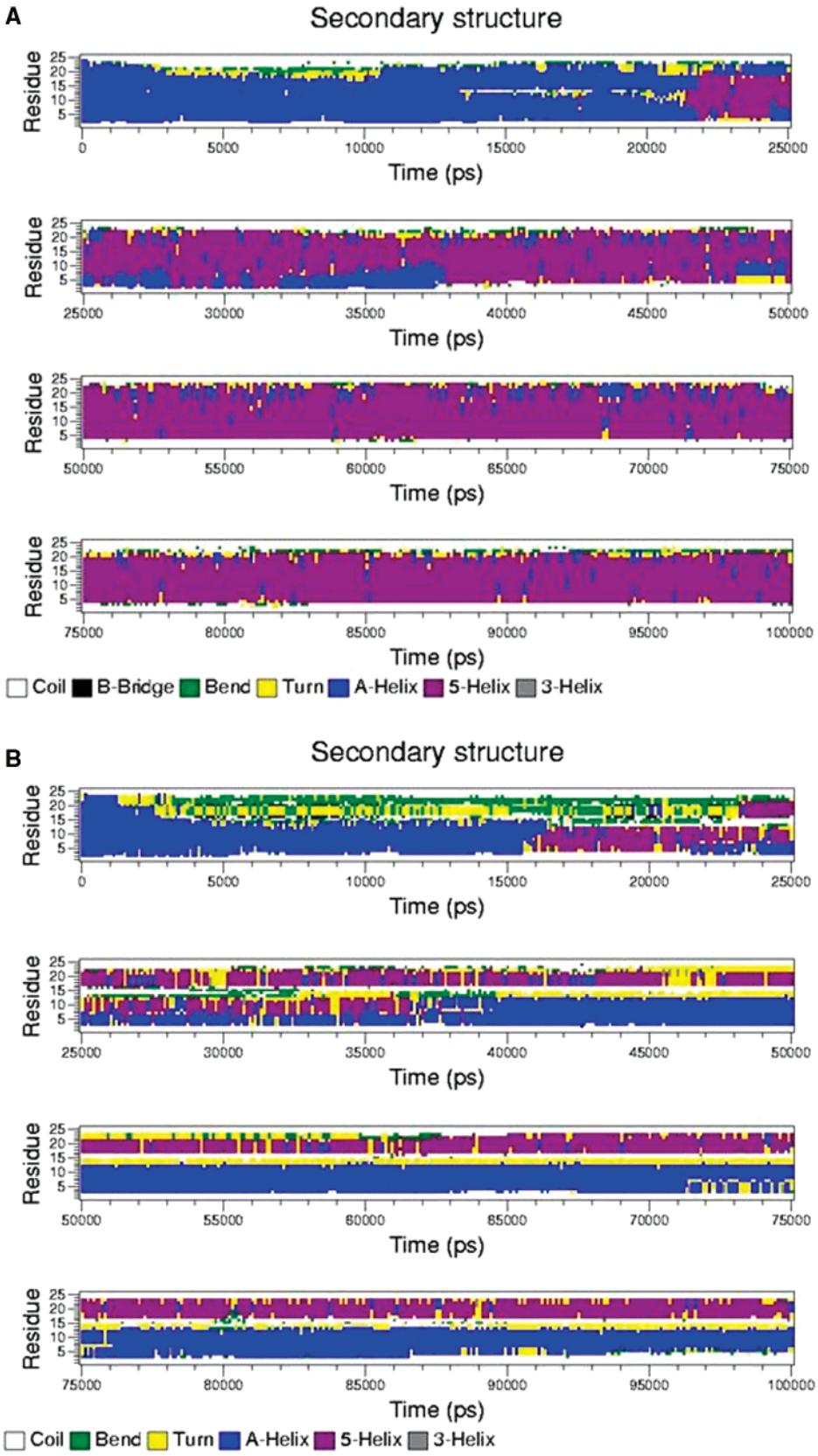

FIGURE 4: Secondary structure analysis of the IQ2 (A) and the IQ4 (B) peptides as a function of the simulation time. The residue number runs along the ordinate and time along the abscissa. Color codes are used to represent secondary structure elements.

gradually loosens up, transforming from an α-helix to a turn, which propagates to a 5-helix structure. What merits notice is that the very same region of the IQ4 sequence, between residues 14 to 19, can harbor a kink when the peptide is allowed to relax in aqueous media. The common location of the kink at both the IQ4 and the extended IQ4 peptides suggests that the intrinsic hinge and inherent flexibility are innate, rather than a simulation's relic. Moreover, when the

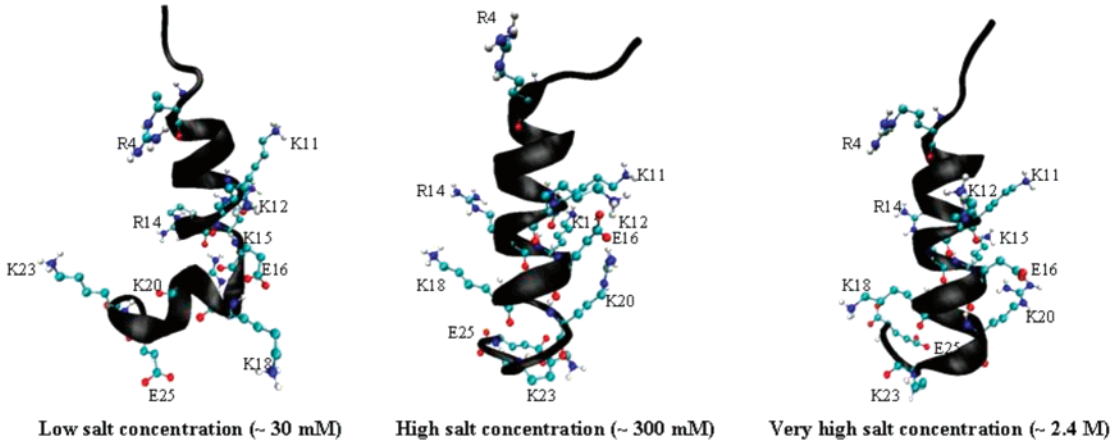

FIGURE 5: Snapshots of the simulated structures of the IQ4 peptide at different salt concentrations. Left: After 20-ns simulation at low salt concentration (~30 mM). Middle: After 100-ns simulation at high salt concentration (~300 mM). Right: After 100 ns at very high salt concentration (~2.4 mM). Charged residues (R4, K11, K12, R14, K15, E16, K18, R20, K23 and E25) are shown as indicatives.

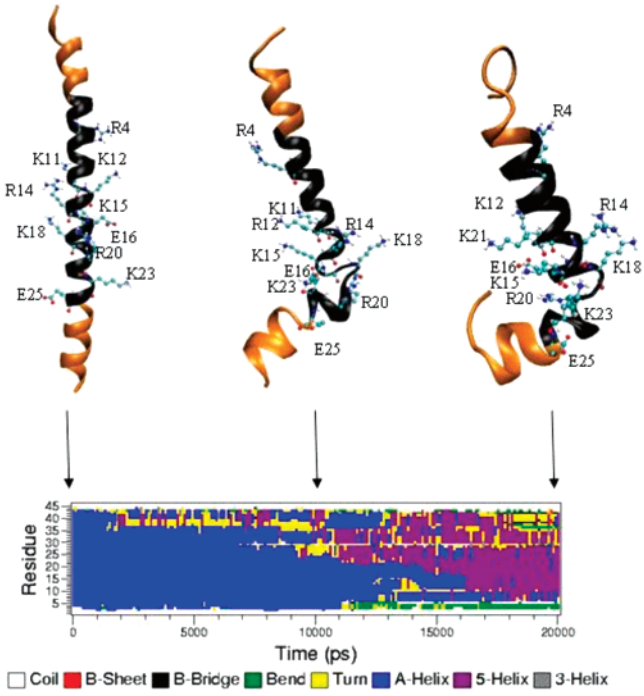

FIGURE 6: Secondary structure analysis of the extended IQ4 peptide as a function of the simulation time. The residue number runs along the ordinate and time along the abscissa. Color codes are used to represent secondary structure elements. Representative snapshots of the peptide, in which the added residues and the peptide are colored in orange, are shown every 10 ns. Charged residues of the IQ4 peptide (R4, K11, K12, R14, K15, E16, K18, R20, K23 and E25) are shown as indicatives.

RMSF was calculated for the IQ4 peptide's simulations (data not shown), it turned out that residues that present high RMSF values correspond to those that curve.

DISCUSSION

Computational studies of large macromolecular assemblages have come a long way during the past 10 years. With the explosion of computer power and parallel computing, time scales of MD simulations have been substantially extended. However, limitations remain for studies of large-scale conformational changes occurring on time scales beyond nanoseconds, especially for large macromolecules such as myosin. Hence, instead of simulating the entire myosin molecule, we concentrated on its neck domain. Nevertheless, the conclusions and their implications may hold for the mechanochemical walking mechanism of myosin V since its neck domain is an autonomous independent region, clearly separated from the head and the tail.

On this study, which to our knowledge is the first to investigate the dynamics of the myosin's neck, we describe a usage of the MD methodology as a tool to analyze the structures of the IQ peptides from the yeast *Saccharomyces cerevisiae* outside their crystal lattice, in an aqueous environment. Since none of the IQ peptides was crystallized in the absence of the light chain protein Mlc1p, their initial structures were derived from the published crystal structures of the Mlc1p−IQ protein−peptide complexes (*47*). Considering the relatively long duration of our simulations (total of 0.47 μs) and the repetitive pattern of the structures obtained at different simulations' conditions, we propose that the predicted structures of both IQ peptides represent their stable MD-derived solution conformations.

Comparison of the two IQ peptides' MD trajectories and their secondary structure analysis reveal that both IQ peptides explore the conformational space until stable configurations emerge. The IQ2 peptide maintains a stable rigid rodlike structure during MD simulation, though it loses most of its α-helical features at the expense of gaining a 5-helix structure. On the contrary, the IQ4 peptide abruptly modifies its shape from an elongated α-helix into a helix−loop−helix conformation through intermediate states, being less stiff and tending to curve and flex in a profound manner. Its secondary structure analysis reveals a newly appearing 5-helix and coil/turn configurations that occupy about ~50% of its secondary structure, whereas its other half still attains the initial α-helix content.

The MD-derived state of the IQ4 peptide is energetically favorable over its X-ray structure. The difference between the MD-derived structures of the two peptides may be attributed to the higher net charge of the IQ4 peptide ($Z = +6$) than that of the IQ2 peptide ($Z = +2$), and is reflected by the electrostatic attraction between positive and negative residues located on its N- and C-termini (for example, R4-E25). In contrast, the IQ4 peptide presents an intrinsic instability and an increased tendency to flex since its MD-derived structure appears to be influenced by the ionic strength of its environment.

Table 2: The Sequence of the LCBD (poly-IQ) of Myosin V Myo2p (Swiss-Prot Entry P19524)[a]

	Sequence	Total Charge
IQ1	^{784}MHNSIVMIQKKIRAKYYRKQYL^{805}	+6
IQ2	^{806}QISQAIKYLQNNIKGFIIRQRVNDE^{830}	+2
IQ3	^{831}MKVNCATLLQAAYRGHSIRANVF^{853}	+3
IQ4	^{854}SVLRTITNLQKKIRKELKQRQLKQE^{878}	+6
IQ5	^{879}HEYNAAVTIQSKVRTFEPRSRFL^{901}	+2
IQ6	^{902}RTKKDTVVVQSLIRRRAAQRKLKQL^{926}	+8

[a] Positive and negative residues are colored by blue and red, respectively.

The simulations of the IQ4 peptide at increasing salt concentrations imply that its charged residues take a major role in the refolding process of the peptide. This supplies a framework for design of *in vivo* mutants that will address this question. In addition, these simulations of the IQ4 peptide at increasing salt concentrations exemplify how crystallographic conditions may determine the outcome structure of the crystal. The IQ4 peptide presents a curved shape when simulated under subphysiological and physiological salt concentrations (~30 mM and ~100 mM), which was not detected when the simulations were performed under overphysiological salt concentrations (~300 mM and ~2.4 M). At ionic strengths of ~300 mM and above, there is a strong influence of the screening electrolyte on the conformation of the IQ4 peptide and the Debye−Hückel effect is stressed. That precludes the IQ4 peptide from bending, keeping it as a straight α-helix. Apparently, as indicated by this study, the crystalline structure of the IQ4 peptide was imposed by specific crystallographic conditions of its crystallization buffer liquor (such as its salt concentration and ionic strength). Fundamental deviations of X-ray determined structures from native configurations of proteins were documented, as well, in other cases (*68*−*70*).

The bent IQ4 peptide's structure is too short for searching for similar features in other proteins except myosins, and hence evaluating of its properties is limited to the simulations reported in the present study. The main property of the IQ4 sequence is a plethora of charged residues when compared to the other Myo2p IQ peptides (Table 2). The main characteristic of the bending location seems to be clustering of positive residues in the sequence at a configuration that packs the charges into a tight knot when the structure is straight, and allows them to spread in the bent configuration (see Figure 2A). Indeed, the comparison of the electrostatic and the LJ potentials, as they vary with time, reveals an initial electrostatic relaxation that precedes the LJ stabilization, only to be followed by a longer extended minimization of the electrostatic potential. In accord with this interpretation, we observe that once the ionic screening is intensified, the IQ4 peptide retains its rodlike structure.

The peptides that are found at the periphery of the LCBD, namely, IQ1 and IQ6, are highly charged and may be prone to be bent. However, attempts to predict the structures of these peptides are not of high structural or functional relevance since they are directly connected to the head and tail domains of the myosin, respectively. Yet, we can predict the conformations of the IQ2−IQ5 peptides based on charge and sequence considerations, published X-ray structures (PDB: 1M45, 1M46 and 1N2D) and MD simulations ((*41*, *42*) and the current research). From the IQ2, IQ3, IQ4 and IQ5 peptides, the IQ4 peptide is the most charged. It bears eight positive and two negative residues, probably contributing to its internal elasticity and flexibility. The other IQ peptides are less charged and possess only a few charged residues (2−3). Hence, from a sequence and charge perspective, we conclude that the IQ2, IQ3 and IQ5 peptides would keep an elongated conformation together with their counterpart light chain proteins. This is corroborated by X-ray structures of the Mlc1p−IQ2 (PDB: 1M45) and the Mlc1p−IQ2/3 (PDB: 1N2D) complexes, in which the peptides maintain a rigid helical structure. Considering our extensive MD simulations presented in this study, the IQ2 peptide does actually maintain a straight a rodlike conformation, whereas the IQ4 tends to bend and flex.

Myosin V moves via a hand-over-hand mechanism, where its motor domain takes steps of ~36 nm. The conversion of the torque into a long striding motion is attained by its neck domain, in which the linear α-helical poly-IQ sequence is supplemented by corresponding wrapping CaM-like proteins. In order to convert the torque into motion, the lever arm should keep a straight configuration so that the translational motion will be maximized. However, the sequential stepping events of myosin are associated with alteration of the angle between its lever arm and motor head, with a feedback mechanism affecting the affinity of the head to the actin filament (*25*). The uneven mode of these forces along the lever arm appears to affect the neck's CaM-like proteins saturated shape. Consequently, a mechanical internal stress, associated with the mechanochemical function of the myosin molecule, is generated. This internal strain induces curvature of the leading lever arm's LCBD at a defined location, as suggested by microscopy (*15*−*24*), mathematical and kinetic modeling (*25*−*29*), and optical trapping (*30*, *31*) of myosin. The appearance of a curved arm with a bent elbow at its mid-section affects the spatial interactions between the motor head and the lever arm, and the properties of the ratchet locking (*25*).

Our observations about the dynamics of the IQ peptides allow for a dynamic functional model of myosin V's LCBD from the budding yeast *Saccharomyces cerevisiae*. Consistent with the elastic nature of the LCBD and the dynamic characteristic of the lever arm mechanism, we suggest that

Table 3: Sequences of the LCBD of Class V Myosins from Yeast (Myo2p_Sc and Myo4p_Sc), Mouse (MyoVa_Mo), Rat (MyoVa_Ra) and Human (MyoVa_Hu)[a]

	IQ1	IQ2
Myo2p_Sc	^{784}MHNSIVMIQKKIRAKYYRKQYLQISQAIKYLQNNIKGFIIRQRVNDE^{830}	
Myo4p_Sc	^{780}MNEICIIIQKKIRARYYRLQYLQTMESIKKCQSQIRSLLVRTRVDHE^{826}	
MyoVa_Mo	^{766}LRAACIRIQKTIRGWLLRKRYLCMQRAAITVQRYVRGYQARCYAKFL^{812}	
MyoVa_Ra	^{766}LRAACIRIQKTIRGWLLRKRYLCMQRAAITVQRYVRGYQARCYAKFL^{812}	
MyoVa_Hu	^{766}LRAACIRIQKTIRGWLLRKKYLRMRKAAITMQRYVRGYQARCYAKFL^{812}	

	IQ3	IQ4
Myo2p_Sc	^{831}MKVNCATLLQAAYRGHSIRANVFSVLRTITNLQKKIRKELKQRQLKQE^{878}	
Myo4p_Sc	^{827}LKTRAAILLQTNIRALWKREYYRAAIGQIIKLQCTCKRKLILDSVNRK^{874}	
MyoVa_Mo	^{813}RRTKAATTIQKYWRMYVVRRRYKIRRAATIVIQSYLRGYLTRNRYRKI^{860}	
MyoVa_Ra	^{813}RRTKAATTIQKYWRMYVVRRKYKIRRAATIVLQSYLRGYLARNRYRKI^{860}	
MyoVa_Hu	^{813}RRTKAATIIQKYWRMYVVRRRYKIRRAATIVLQSYLRGFLARNRYRKI^{860}	

	IQ5	IQ6
Myo2p_Sc	^{881}HEYNAAVTIQSKVRTFEPRSRFLRTKKDTVVVQSLIRRRAAQRKLKQL^{926}	
Myo4p_Sc	^{875}VNRKFMLMAAVIIQSYIRSYGHKTDYRTLKRSSILVQSAMRMQLARRR^{922}	
MyoVa_Mo	^{861}HYKRTMKAIVYLQCCFRRMMAKRDVKKLKIEARSVERYKKLHIGMENK^{908}	
MyoVa_Ra	^{861}LREHKAVIIQKRVRGWLARTHYKRTMKAIIYLQCCFRRMMAKRELKKL^{908}	
MyoVa_Hu	^{861}LREHKAVIIQKRVRGWLARTHYKRSMHAIIYLQCCFRRMMAKRELKKL^{908}	

[a] The peptides (IQ1−IQ6) are colored by red, blue, green, black, pink and turquoise, respectively. Swiss-Prot accession numbers are Myo2p_Sc (P19524), Myo4p_Sc (P32492), MyoVa_Mo (Q99104), MyoVa_Ra (Q9QYF3) and MyoVa_Hu (Q9Y4I1). Charged residues are underlined.

the banana-shaped conformation formed by myosin's arm is generated through the IQ4 peptide that presents an intrinsic inner characteristic to flex and curve in solution. This is in accordance with the secondary structure analysis of the IQ2 and the IQ4 peptides, in which the former peptide completely transforms into a 5-helix conformation whereas the latter peptide harbors a coil between an α-helix and 5-helix conformations. Thus, the secondary structure of the IQ2 peptide prevents it from bending, while that of the Myo2p IQ4 peptide allows it to bend and curl. The hinge shown at the neck's IQ4 peptide's conformation, observed in all our simulations under physiological salt conditions (and also for the extended IQ4 peptide), may correspond to the bent solution state of the lever arm of myosin. Our proposed model is supported by previous studies (*41*, *42*), in which we found that, in the presence of the Mlc1p protein, the IQ4 peptide loses its rodlike shape while the IQ2 peptide keeps it. In this fashion, the Mlc1p protein does not hinder the capacity of the IQ4 peptide to bend in the very same location when simulated in its absence. Interestingly, further supporting data was supplied by fluorescence and near- and far-UV CD measurements, where it was found that a murine myosin IQ3/4 double-length sequence cannot exist as a continuous straight helix (*71*), even in the presence of CaM.

As indicated by the MD simulations of the IQ4 peptide at different salt concentrations, at a physiological salt concentration (∼150 mM) it should be able to naturally switch from a bent to a rodlike configuration. This suggests that relatively minor forces are needed in order to induce its *in vivo* alternation between the two conformation states. Therefore, the poly-IQ sequence may be bent at the IQ4 peptide region that functions as a joint since its conformational process of refolding is crucial to the myosin's walking over the actin filament. Apparently, the bended elbow conformation of the LCBD's lead arm, which is suggested to be caused by the curved IQ4 peptide, is a fundamental element in the myosin's mechanochemical movement mechanism.

The uniqueness of the IQ4 peptide is not restricted to the yeast Myo2p, but rather is a common feature for class V myosins from different species (Table 3). Among the poly-IQ sequence of yeast, mouse rat and human, the IQ4 peptide carries the highest number of charged residues (7−10) as compared to the other IQ peptides. Evidently, the high number of charged residues is evolutionarily conserved, and

this may indicate that our suggestion about the intrinsic capacity of the IQ4 peptide to bend can be valid for class V myosins from vertebrates as well.

An essential point for mechanical force generation in myosin systems is how the energy released by ATP hydrolysis in the myosin motor domain gives rise to the movement of the myosin head along the actin filament. By performing MD simulations of the motor domain of myosin S1, Minami and co-workers (*32*) suggest that the energy released by the ATP hydrolysis is transformed into kinetic energy of atoms located around the nucleotide-binding site pocket found in the motor domain. Their analysis indicates that the structural deformation, which is caused by the ATP hydrolysis, extends over the motor domain core. It spreads and induces varying collective motions of atoms at the actin-binding site, and simultaneously, at the junction with the neck. Our simulations may complement this study by suggesting that the influence of the torque produced by ATP hydrolysis may not cease at the nucleotide-binding site located at the motor domain, but rather continues to move and be transferred along the myosin molecule through its neck at the direction of the tail. Evidently, this motion induces bending of the IQ4 peptide, which consequently enables the myosin's neck to flex.

The functional model of myosin V's LCBD from the budding yeast *Saccharomyces cerevisiae*, as presented here, may be valid only whether the yeast's myosin V motor is processive. This issue is under current dispute and no clear proof, so far, conclusively solved the puzzle. Mooseker and co-workers (*13*) claim that the yeast's class V myosins Myo2p and Myo4p are nonprocessive *in vitro*. Their conclusion is based upon *in vitro* indirect assays, in which the myosin's velocity and landing rate on the actin filament, as they varied with the myosin's motor domain density, were followed. However, the authors did not exclude the possibility of *in vivo* processivity. An explanation for the absence of processivity in their study may be that the yeast class V myosins are processive due to a regulatory event and in its absence are nonprocessive. It was shown that binding of the dynactin multi-subunit protein complex to the microtubule motors dynein (*72*, *73*) and kinesin (*74*) increases their processivity. Since myosin, dynein and kinesin are all molecular motors, it is likely the myosin's function is regulated by dynactin or another regulating factor. Furthermore, Trybus and co-workers (*14*) dealt with the yeast's myosin V lack of processivity in a recent publication, suggesting that the yeast Myo4p molecule can exist either as a nonprocessive monomer or a processive dimer, depending on the conditions. A high identity (34%) and similarity (58%) between the LCBDs of Myo2p and Myo4p, as calculated by BLAST (*75*, *76*), lead to the conclusion that most probably both share similar features. It should be noted that a monomer−dimer equilibrium that impacts on processivity has been proposed to exist at class VI myosins (for a review, see (*77*)), and it is possible that this may be a general mechanism for regulating *in vivo* processivity. Additionally, the research of Trybus and co-workers proposes that native yeast Myo4p is nonprocessive (or weakly processive) at a high ionic strength and more processive at a physiological ionic strength. Our observations are in favor of the findings raised by Trybus and co-workers, suggesting that at a physiological salt concentration the IQ4 peptide is able to bend but high salt conditions prevent it from flexing. In other words, when the conditions enable, the myosin V molecule dimerizes and becomes processive; and *vice versa*, when the conditions are unfavorable, the molecule cannot dimerize and hence may present monomeric nonprocessive characteristics.

The interaction between the IQ peptides and their corresponding CaM-like protein along the LCBD is a complex function, reflecting the local protein−peptide interactions and the interactions between the light-chain proteins, one with the others. It is likely that the relative motion of the motor domain, with respect to the lever arm, imposes a stress not only on the LCBD but also on the CaM-like proteins that are threaded along it. The double path of the stress along the α-helix and wrapping proteins may provide a mechanism that regulates the flexing point along the lever arm, facilitating the transfer of the local torque into effective translational motion of the whole, double-headed protein. Thus, by careful analysis of data combining (i) MD simulations of the motor (*32*) and the neck ((*41*, *42*) and this study) domains of myosin and (ii) single molecule experiments of chimeric class V myosins, we offer an additional piece to the mechanochemical walking mechanism puzzle of myosin V. Obviously, additional experimental and theoretical work is required to fully elucidate the mechanism of myosin V motions.

REFERENCES

1. Reck-Peterson, S. L., Provance, D. W., Jr., Mooseker, M. S., and Mercer, J. A. (2000) Class V myosins, *Biochim. Biophys. Acta 1496*, 36−51.
2. Kalhammer, G., and Bahler, M. (2000) Unconventional myosins, *Essays Biochem. 35*, 33−42.
3. Nascimento, A. A., Cheney, R. E., Tauhata, S. B., Larson, R. E., and Mooseker, M. S. (1996) Enzymatic characterization and functional domain mapping of brain myosin-V, *J. Biol. Chem. 271*, 17561−17569.
4. Langford, G. M. (2002) Myosin-V, a versatile motor for short-range vesicle transport, *Traffic 3*, 859−865.
5. Sellers, J. R., and Veigel, C. (2006) Walking with myosin V, *Curr. Opin. Cell Biol. 18*, 68−73.
6. Rayment, I., Holden, H. M., Whittaker, M., Yohn, C. B., Lorenz, M., Holmes, K. C., and Milligan, R. A. (1993) Structure of the actin-myosin complex and its implications for muscle contraction, *Science 261*, 58−65.
7. Mehta, A. D., Rock, R. S., Rief, M., Spudich, J. A., Mooseker, M. S., and Cheney, R. E. (1999) Myosin-V is a processive actin-based motor, *Nature 400*, 590−593.
8. Geeves, M. A., and Holmes, K. C. (1999) Structural mechanism of muscle contraction, *Annu. Rev. Biochem. 68*, 687−728.
9. Langford, G. M., Kuznetsov, S. A., Johnson, D., Cohen, D. L., and Weiss, D. G. (1994) Movement of axoplasmic organelles on actin filaments assembled on acrosomal processes: evidence for a barbed-end-directed organelle motor, *J. Cell Sci. 107* (Part 8), 2291−2298.
10. Sakamoto, T., Wang, F., Schmitz, S., Xu, Y., Xu, Q., Molloy, J. E., Veigel, C., and Sellers, J. R. (2003) Neck length and processivity of myosin V, *J. Biol. Chem. 278*, 29201−29207.
11. Brockerhoff, S. E., Stevens, R. C., and Davis, T. N. (1994) The unconventional myosin, Myo2p, is a calmodulin target at sites of cell growth in Saccharomyces cerevisiae, *J. Cell Biol. 124*, 315−323.
12. Haarer, B. K., Petzold, A., Lillie, S. H., and Brown, S. S. (1994) Identification of MYO4, a second class V myosin gene in yeast, *J. Cell Sci. 107* (Part 4), 1055−1064.
13. Reck-Peterson, S. L., Tyska, M. J., Novick, P. J., and Mooseker, M. S. (2001) The yeast class V myosins, Myo2p and Myo4p, are nonprocessive actin-based motors, *J. Cell Biol. 153*, 1121−1126.
14. Krementsova, E. B., Hodges, A. R., Lu, H., and Trybus, K. M. (2006) Processivity of chimeric class V myosins, *J. Biol. Chem. 281*, 6079−6086.
15. Nguyen, H., and Higuchi, H. (2005) Motility of myosin V regulated by the dissociation of single calmodulin, *Nat. Struct. Mol. Biol. 12*, 127−132.

16. Toprak, E., Enderlein, J., Syed, S., McKinney, S. A., Petschek, R. G., Ha, T., Goldman, Y. E., and Selvin, P. R. (2006) Defocused orientation and position imaging (DOPI) of myosin V, *Proc. Natl. Acad. Sci. U.S.A. 103*, 6495−6499.
17. Syed, S., Snyder, G. E., Franzini-Armstrong, C., Selvin, P. R., and Goldman, Y. E. (2006) Adaptability of myosin V studied by simultaneous detection of position and orientation, *EMBO J. 25*, 1795−1803.
18. Sakamoto, T., Yildez, A., Selvin, P. R., and Sellers, J. R. (2005) Step-size is determined by neck length in myosin V, *Biochemistry 44*, 16203−16210.
19. Lu, H., Krementsova, E. B., and Trybus, K. M. (2006) Regulation of myosin V processivity by calcium at the single molecule level, *J. Biol. Chem. 281*, 31987−31994.
20. Dunn, A. R., and Spudich, J. A. (2007) Dynamics of the unbound head during myosin V processive translocation, *Nat. Struct. Mol. Biol. 14*, 246−248.
21. Burgess, S., Walker, M., Wang, F., Sellers, J. R., White, H. D., Knight, P. J., and Trinick, J. (2002) The prepower stroke conformation of myosin V, *J. Cell Biol. 159*, 983−991.
22. Walker, M. L., Burgess, S. A., Sellers, J. R., Wang, F., Hammer, J. A., 3rd, Trinick, J., and Knight, P. J. (2000) Two-headed binding of a processive myosin to F-actin, *Nature 405*, 804−807.
23. Volkmann, N., Liu, H., Hazelwood, L., Krementsova, E. B., Lowey, S., Trybus, K. M., and Hanein, D. (2005) The structural basis of myosin V processive movement as revealed by electron cryomicroscopy, *Mol. Cell 19*, 595−605.
24. Yildiz, A., Forkey, J. N., McKinney, S. A., Ha, T., Goldman, Y. E., and Selvin, P. R. (2003) Myosin V walks hand-over-hand: single fluorophore imaging with 1.5-nm localization, *Science 300*, 2061−2065.
25. Lan, G., and Sun, S. X. (2005) Dynamics of myosin-V processivity, *Biophys. J. 88*, 999−1008.
26. Lan, G., and Sun, S. X. (2006) Flexible Light-Chain and Helical Structure of F-Actin Explain the Movement and Step Size of Myosin-VI, *Biophys. J. 91*, 4002−4013.
27. Skau, K. I., Hoyle, R. B., and Turner, M. S. (2006) A kinetic model describing the processivity of myosin-V, *Biophys. J. 91*, 2475−2489.
28. Smith, D., and Sleep, J. (2006) Strain-dependent kinetics of the Myosin working stroke, and how they could be probed with optical-trap experiments, *Biophys. J. 91*, 3359−3369.
29. Smith, D. A., and Sleep, J. (2004) Mechanokinetics of rapid tension recovery in muscle: the Myosin working stroke is followed by a slower release of phosphate, *Biophys. J. 87*, 442−456.
30. Purcell, T. J., Sweeney, H. L., and Spudich, J. A. (2005) A force-dependent state controls the coordination of processive myosin V, *Proc. Natl. Acad. Sci. U.S.A. 102*, 13873−13878.
31. Veigel, C., Schmitz, S., Wang, F., and Sellers, J. R. (2005) Load-dependent kinetics of myosin-V can explain its high processivity, *Nat. Cell Biol. 7*, 861−869.
32. Kawakubo, T., Okada, O., and Minami, T. (2005) Molecular dynamics simulations of evolved collective motions of atoms in the myosin motor domain upon perturbation of the ATPase pocket, *Biophys. Chem. 115*, 77−85.
33. Koppole, S., Smith, J. C., and Fischer, S. (2006) Simulations of the myosin II motor reveal a nucleotide-state sensing element that controls the recovery stroke, *J. Mol. Biol. 361*, 604−616.
34. Lawson, J. D., Pate, E., Rayment, I., and Yount, R. G. (2004) Molecular dynamics analysis of structural factors influencing back door pi release in myosin, *Biophys. J. 86*, 3794−3803.
35. Mesentean, S., Koppole, S., Smith, J. C., and Fischer, S. (2007) The principal motions involved in the coupling mechanism of the recovery stroke of the myosin motor, *J. Mol. Biol. 367*, 591−602.
36. Okimoto, N., Yamanaka, K., Ueno, J., Hata, M., Hoshino, T., and Tsuda, M. (2001) Theoretical studies of the ATP hydrolysis mechanism of myosin, *Biophys. J. 81*, 2786−2794.
37. Woo, H. J. (2007) Exploration of the conformational space of myosin recovery stroke via molecular dynamics, *Biophys. Chem. 125*, 127−137.
38. Yu, H., Ma, L., Yang, Y., and Cui, Q. (2007) Mechanochemical Coupling in the Myosin Motor Domain. I. Insights from Equilibrium Active-Site Simulations, *PLoS Comput. Biol. 3*, e21.
39. Yu, H., Ma, L., Yang, Y., and Cui, Q. (2007) Mechanochemical Coupling in the Myosin Motor Domain. II. Analysis of Critical Residues, *PLoS Comput. Biol. 3*, e23.
40. Liu, Y., Scolari, M., Im, W., and Woo, H. J. (2006) Protein-protein interactions in actin-myosin binding and structural effects of R405Q mutation: a molecular dynamics study, *Proteins 64*, 156−166.
41. Ganoth, A., Nachliel, E., Friedman, R., and Gutman, M. (2006) Molecular dynamics study of a calmodulin-like protein with an IQ peptide: Spontaneous refolding of the protein around the peptide, *Proteins 64*, 133−146.
42. Ganoth, A., Friedman, R., Nachliel, E., and Gutman, M. (2006) A molecular dynamics study and free energy analysis of complexes between the Mlc1p protein and two IQ motif peptides, *Biophys. J. 91*, 2436−*2450*.
43. Berendsen, H. J. C., van der Spoel, D., and van Drunen, R. (1995) GROMACS: A message-passing parallel molecular dynamics implementation, *Comput. Phys. Commun. 91*, 43−56.
44. Lindahl, E., Hess, B., and van der Spoel, D. (2001) Gromacs 3.0: A package for molecular simulation and trajectory analysis, *J. Mol. Model. 7*, 306−317.
45. van Der Spoel, D., Lindahl, E., Hess, B., van Buuren, A. R., Apol, E., Meulenhoff, P. J., Tieleman, D. P., Sijbers, A. L. T. M., Feenstra, A. K., van Drunen, R., and Berendsen, H. J. C. (2004) Groningen Machine for Molecular Simulations. BIOSON Research Institute, Groningen, The Netherlands.
46. van Gunsteren, W. F., Billeter, S. R., Eising, A. A., Hunenberger, P. H., Kruger, P., Mark, A. E., Scott, W. R. P., and Tironi, I. G. (1996) *Biomolecular Simulation: The GROMOS96 Manual and User Guide*, Vdf Hochschulverlag AG an der ETH Zurich, Zurich, pp 1−1024.
47. Terrak, M., Otterbein, L. R., Wu, G., Palecanda, L. A., Lu, R. C., and Dominguez, R. (2002) Crystallization, X-ray characterization and selenomethionine phasing of Mlc1p bound to IQ motifs from myosin V, *Acta Crystallogr, Sect. D: Biol. Crystallogr. 58*, 1882−1885.
48. Berman, H. M., Battistuz, T., Bhat, T. N., Bluhm, W. F., Bourne, P. E., Burkhardt, K., Feng, Z., Gilliland, G. L., Iype, L., Jain, S., Fagan, P., Marvin, J., Padilla, D., Ravichandran, V., Schneider, B., Thanki, N., Weissig, H., Westbrook, J. D., and Zardecki, C. (2002) The Protein Data Bank, *Acta Crystallogr., Sect. D: Biol. Crystallogr. 58*, 899−907.
49. Berendsen, H. J. C., Postma, J. P. M., van Gunsteren, W. F., and Hermans, J. (1969) Interaction Models for Water in Relation to Protein Hydration, *Nature 224*, 175−177.
50. Hess, B., Bekker, H., Berendsen, H. J. C., and Fraaije, J. G. E. M. (1997) LINCS: A linear constraint solver for molecular simulations, *J. Comput. Chem. 18*, 1463−1472.
51. Miyamoto, S., and Kollman, P. A. (1992) SETTLE: An Analytical Version of the SHAKE and RATTLE Algorithms for Rigid water models, *J. Comput. Chem. 13*, 952−962.
52. Berendsen, H. J. C., Postma, J. P. M., DiNola, A., and Haak, J. R. (1984) Molecular dynamics with coupling to an external bath, *J. Chem. Phys. 81*, 3684−3690.
53. Essman, U., Perela, L., Berkowitz, M. L., Darden, T., Lee, H., and Pederse, L. G. (1995) A smooth particle mesh Ewald method, *J. Chem. Phys. 103*, 8577−8592.
54. Humphrey, W., Dalke, A., and Schulten, K. (1996) VMD: visual molecular dynamics, *J. Mol. Graphics 14*, 33 38, 27 38.
55. Daidone, I., Amadei, A., and Di Nola, A. (2005) Thermodynamic and kinetic characterization of a beta-hairpin peptide in solution: an extended phase space sampling by molecular dynamics simulations in explicit water, *Proteins 59*, 510−518.
56. Tavernelli, I., Cotesta, S., and Di Iorio, E. E. (2003) Protein dynamics, thermal stability, and free-energy landscapes: a molecular dynamics investigation, *Biophys. J. 85*, 2641−*2649*.
57. Amadei, A., Linssen, A. B., de Groot, B. L., van Aalten, D. M., and Berendsen, H. J. (1996) An efficient method for sampling the essential subspace of proteins, *J. Biomol. Struct. Dyn. 13*, 615−625.
58. Cecchini, M., Curcio, R., Pappalardo, M., Melki, R., and Caflisch, A. (2006) A molecular dynamics approach to the structural characterization of amyloid aggregation, *J. Mol. Biol. 357*, 1306−1321.
59. Daidone, I., D'Abramo, M., Di Nola, A., and Amadei, A. (2005) Theoretical characterization of alpha-helix and beta-hairpin folding kinetics, *J. Am. Chem. Soc. 127*, 14825−14832.
60. D'Abramo, M., Rinaldi, A. C., Bozzi, A., Amadei, A., Mignogna, G., Di Nola, A., and Aschi, M. (2006) Conformational behavior of temporin A and temporin L in aqueous solution: a computational/experimental study, *Biopolymers 81*, 215−224.

61. Cecchini, M., Rao, F., Seeber, M., and Caflisch, A. (2004) Replica exchange molecular dynamics simulations of amyloid peptide aggregation, *J. Chem. Phys. 121*, 10748−10756.
62. Onuchic, J. N., Luthey-Schulten, Z., and Wolynes, P. G. (1997) Theory of protein folding: the energy landscape perspective, *Annu. Rev. Phys. Chem. 48*, 545−600.
63. Wales, D. G. (2003) *Energy Landscapes*, Cambridge University Press, Cambridge.
64. Duneau, J. P., Garnier, N., and Genest, M. (1997) Insight into signal transduction: structural alterations in transmembrane helices probed by multi-1 ns molecular dynamics simulations, *J. Biomol. Struct. Dyn. 15*, 555−572.
65. Duneau, J. P., Crouzy, S., Chapron, Y., and Genest, M. (1999) Dynamics of the transmembrane domain of the ErbB-2 receptor, *Theor. Chem. Acc. 101*, 87−91.
66. Shepherd, C. M., van der Spoel, D., and Vogel, H. J. (2004) Molecular dynamics simulations of peptides from the central domain of smooth muscle caldesmon, *J. Biomol. Struct. Dyn. 21*, 555−566.
67. Lee, K. H., Benson, D. R., and Kuczera, K. (2000) Transitions from alpha to pi helix observed in molecular dynamics simulations of synthetic peptides, *Biochemistry 39*, 13737−13747.
68. Eyal, E., Gerzon, S., Potapov, V., Edelman, M., and Sobolev, V. (2005) The limit of accuracy of protein modeling: influence of crystal packing on protein structure, *J. Mol. Biol. 351*, 431−442.
69. DePristo, M. A., de Bakker, P. I., and Blundell, T. L. (2004) Heterogeneity and inaccuracy in protein structures solved by X-ray crystallography, *Structure 12*, 831−838.
70. Steuber, H., Zentgraf, M., Gerlach, C., Sotriffer, C. A., Heine, A., and Klebe, G. (2006) Expect the Unexpected or Caveat for Drug Designers: Multiple Structure Determinations Using Aldose Reductase Crystals Treated under Varying Soaking and Co-crystallisation Conditions, *J. Mol. Biol. 363*, 174−187.
71. Martin, S. R., and Bayley, P. M. (2002) Regulatory implications of a novel mode of interaction of calmodulin with a double IQ-motif target sequence from murine dilute myosin V, *Protein Sci. 11*, 2909−2923.
72. Culver-Hanlon, T. L., Lex, S. A., Stephens, A. D., Quintyne, N. J., and King, S. J. (2006) A microtubule-binding domain in dynactin increases dynein processivity by skating along microtubules, *Nat. Cell Biol. 8*, 264−270.
73. King, S. J., and Schroer, T. A. (2000) Dynactin increases the processivity of the cytoplasmic dynein motor, *Nat. Cell Biol. 2*, 20−24.
74. Berezuk, M. A., and Schroer, T. A. (2007) Dynactin enhances the processivity of kinesin-2, *Traffic 8*, 124−129.
75. Altschul, S. F., Madden, T. L., Schaffer, A. A., Zhang, J., Zhang, Z., Miller, W., and Lipman, D. J. (1997) Gapped BLAST and PSI-BLAST: a new generation of protein database search programs, *Nucleic Acids Res. 25*, 3389−3402.
76. Schaffer, A. A., Aravind, L., Madden, T. L., Shavirin, S., Spouge, J. L., Wolf, Y. I., Koonin, E. V., and Altschul, S. F. (2001) Improving the accuracy of PSI-BLAST protein database searches with composition-based statistics and other refinements, *Nucleic Acids Res. 29*, 2994−3005.
77. Buss, F., Spudich, G., and Kendrick-Jones, J. (2004) Myosin VI: cellular functions and motor properties, *Annu. Rev. Cell Dev. Biol. 20*, 649−676.
78. Guex, N., and Peitsch, M. C. (1997) SWISS-MODEL and the Swiss-PdbViewer: an environment for comparative protein modeling, *Electrophoresis 18*, 2714−2723.

BI701342Y